NANO LETTERS

2008
Vol. 8, No. 6
1602-1609

Space Charge Limited Current Measurements on Conjugated Polymer Films using Conductive Atomic Force Microscopy

Obadiah G. Reid, Keiko Munechika, and David S. Ginger*

Department of Chemistry, University of Washington, Seattle, Washington 98195-1700

Received January 17, 2008; Revised Manuscript Received April 15, 2008

ABSTRACT

We describe local (~150 nm resolution), quantitative measurements of charge carrier mobility in conjugated polymer films that are commonly used in thin-film transistors and nanostructured solar cells. We measure space charge limited currents (SCLC) through these films using conductive atomic force microscopy (c-AFM) and in macroscopic diodes. The current densities we measure with c-AFM are substantially higher than those observed in planar devices at the same bias. This leads to an overestimation of carrier mobility by up to 3 orders of magnitude when using the standard Mott−Gurney law to fit the c-AFM data. We reconcile this apparent discrepancy between c-AFM and planar device measurements by accounting for the proper tip−sample geometry using finite element simulations of tip−sample currents. We show that a semiempirical scaling factor based on the ratio of the tip contact area diameter to the sample thickness can be used to correct c-AFM current−voltage curves and thus extract mobilities that are in good agreement with values measured in the conventional planar device geometry.

Semiconducting polymers are being studied for low cost solar cells, light-emitting diodes, and thin film transistors because they can be deposited from solution at ambient temperature and pressure.[1–5] In particular, a great deal of recent progress has been made in the development of organic photovoltaics. However, the efficiency and stability of even the best organic solar cells are still too low for commercial application.[6–9] Improved performance has been achieved in many applications by optimizing the polymer film morphology;[6–12] nevertheless, exactly how morphology impacts performance is not well-understood. Numerical modeling is a powerful tool for understanding the basic physics of device operation, and while continuum models have had success in reproducing the behavior of many classes of devices,[13–15] the widely recognized importance of nanoscale heterogeneity in semiconducting polymer materials can make direct physical interpretation of continuum models difficult. Indeed, several recent theoretical reports suggest that understanding the effects of nanoscale heterogeneity will be critical if we are to fully understand nanostructured solar cells.[16–20] Therefore, it is important that we develop ways to accurately measure the electronic properties of conjugated polymer films with high resolution, both to serve as inputs to and tests against emerging microscopic device models.

A number of scanning probe microscopy techniques have been employed to probe the morphology and electronic structure of polymer thin film devices. These include electrostatic force microscopy (EFM),[21–24] scanning tunneling microscopy (STM),[25–27] and conductive atomic force microscopy (c-AFM).[28–35] Herein, we focus on c-AFM as a local probe of vertical charge transport because it allows for local current density−voltage measurements ($J-V$) with purely topographic feedback and high resolution. Several groups have used $J-V$ curves measured with c-AFM to extract local hole mobilities, fitting the data with the space charge limited current (SCLC) model.[29,31,33,34,36] However, the extracted values of carrier mobility are often at least an order of magnitude larger than the mobilities[37,38] reported for the same polymers in conventional planar SCLC or time-of-flight measurements.

In this paper, we show that we can use SCLC measurements performed with c-AFM on thin conjugated polymer films to quantitatively determine the local charge carrier mobility. We perform SCLC measurements using both c-AFM and planar devices on films of poly(3-hexylthiophene) (P3HT), poly[2-methoxy-5-(3′,7′-dimethyloctyloxy)-1,4-phenylene vinylene] (MDMO-PPV), and poly-(9,9-dioctylfluorene-co-bis-*N*,*N*-(4-butylphenyl)-bis-*N*,*N*-phenyl-1,4-phenylenediamine (PFB), and we model the current density in both c-AFM and planar device experiments using finite element calculations to account for the electrode

* Corresponding author. E-mail: ginger@chem.washington.edu. Phone: (206) 685-2331. Fax: (206) 685-8665.

10.1021/nl080155l CCC: $40.75
Published on Web 05/01/2008

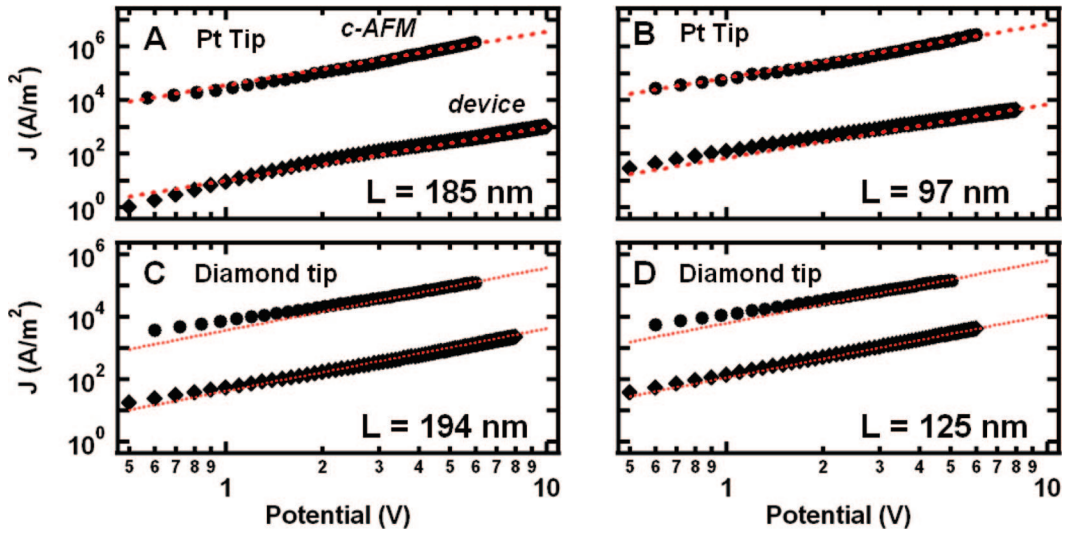

Figure 1. $J-V$ curves measured using c-AFM (circles) and macroscopic devices (diamonds) on various thicknesses of P3HT. Equation 1 is fit to each of the curves (red dotted lines) to extract the mobility. c-AFM measurements were made using a 50 nm diameter platinum coated tips for A,B, while a 250 nm diameter diamond coated tip was used for C,D.

geometry in the c-AFM experiments. We then use our calculations to motivate a semiempirical correction to the Mott−Gurney law based on the ratio of the tip diameter to sample thickness. This correction can account for the difference in geometry between the device and the c-AFM measurements without the need for repeated numerical simulation. Fitting the c-AFM $J-V$ curves with our scaled model yields values of charge carrier mobility that are in agreement with device measurements. We provide a convenient method that can be applied to extract meaningful mobility values without the need for numerical modeling of every sample.

The Mott−Gurney law (eq 1) gives the maximum single-carrier SCLC that can be passed in a planar geometry and is commonly used to fit $J-V$ data from polymer diodes to extract the carrier mobility.[37,39] The Mott−Gurney law is:

$$J = \frac{9}{8}\varepsilon\varepsilon_0\mu\frac{V^2}{L^3} \tag{1}$$

where J is the current density, ϵ is the relative dielectric constant of the active layer, ϵ_0 is the permittivity of free-space, μ is the charge carrier mobility, V is the applied voltage, and L is the thickness of the device. Semiempirical modifications are frequently made to account for the electric field-dependence of the mobility,[40,41] giving:

$$J = \frac{9}{8}\varepsilon\varepsilon_0\mu_0 e^{0.89\gamma\sqrt{V/L}}\frac{V^2}{L^3} \tag{2}$$

where μ_0 is the zero-field mobility and γ expresses the strength of the field-dependence. However, recent studies have suggested that much of the apparent field dependence of the mobility can be explained on a more physically relevant basis in terms of a carrier density dependence.[42] Equation 1 in particular has been used to analyze c-AFM data, and we examine the validity of this approach in detail below.

We performed c-AFM and device measurements on conjugated polymer films of varying thicknesses. The films were prepared by spin-coating warm (45 °C) polymer/chlorobenzene solutions onto a substrate comprising a 100 nm thick indium tin oxide layer (Thin Film Devices Inc.), coated with a 40 nm layer of poly(ethylenedioxythiophene): polystyrenesulfonate (PEDOT:PSS) (Baytron P VP Al 4083). The PEDOT:PSS layer was annealed under N_2(g) at ∼150 °C for 1 h before spin-coating the polymers. All devices were held under dynamic vacuum (∼1 × 10^{-6} mBar) for 12+ hours to remove residual solvent before thermal evaporation of the metal top contact. Our conjugated polymers were obtained from Reike Metals, American Dye Source, and synthesized in-house, for P3HT, PFB, and MDMO-PPV, respectively.

We made conventional hole-only SCLC measurements on planar devices using thermally evaporated gold electrodes. All $J-V$ curves for the planar devices were acquired under vacuum (<10 mB) with a source-measure unit (Keithley Instruments, model 2000). We performed c-AFM experiments using platinum-, diamond-, and gold-coated silicon cantilevers [NanoSensors Inc. (CPP-ContPt and CDT-ContR, spring constant k = 0.2 N/m); Budget Sensors Inc. (BS-ContGB spring constant k = 0.2 N/m)]. c-AFM measurements were performed on the same samples as bulk device measurements in between the evaporated gold electrodes. We used an Asylum Research MFP-3D AFM equipped with an ORCA current preamplifier and a nitrogen flow cell to perform all c-AFM measurements in dry nitrogen.

Figure 1 shows a series of current density−voltage ($J-V$) curves obtained from planar hole-only devices and from c-AFM measurements on P3HT films. Films of two different thicknesses were used for each set of experiments. We acquired the data in Figure 1A,B, using an ∼50 nm diameter platinum tip, and we acquired the data in Figure 1C,D using an ∼250 nm diameter conductive diamond tip. For all of our experiments, we determined the contact area between the tip and the sample assuming ∼1 nm of tip indentation for the platinum and gold tips, which are hemispherical in shape. For the platinum tip used for Figure 1, this results in

Table 1. Average Mobility Values Obtained by Fitting Eq 2 to the Experimental $J-V$ Curves for Each Polymer Using Planar Devices

polymer	μ_0 [cm^2 V^{-1} s^{-1}]	γ [V$^{-1/2}$ m$^{1/2}$]
P3HT	8.3×10^{-5}	0
MDMO-PPV	1.5×10^{-7}	5.4×10^{-4}
PFB	2.3×10^{-7}	7.2×10^{-4}

Table 2. Example Mobility Values Obtained by Fitting Eq 1 to the Experimental $J-V$ Curves Obtained for P3HT ($\gamma = 0$)[a]

AFM tip	L (nm)	μ_{device} [cm^2 V^{-1} s^{-1}]	$\mu_{c\text{-}AFM}$ [cm^2 V^{-1} s^{-1}]	$\mu_{c\text{-}AFM}/\mu_{device}$
platinum	185	2.12×10^{-5}	7.77×10^{-2}	3661
	97	2.19×10^{-5}	2.15×10^{-2}	985
diamond	194	8.45×10^{-5}	9.64×10^{-3}	114
	125	7.38×10^{-5}	4.37×10^{-3}	59

[a] The mobility we extract from our c-AFM measurements is 50−4000 times larger than the values from planar device measurements. Additionally, the c-AFM mobility depends strongly on sample thickness and tip diameter, suggesting that use of eqs 1 or 2 to fit the c-AFM data is inappropriate.

a circular contact patch with a 14 nm diameter. For the diamond tips, which are irregularly shaped, we estimated the contact patch diameter directly from examination of SEM images of the tip (Figure 4A), resulting in a 125 nm diameter patch for the diamond tip used to collect the data in Figure 1. For all c-AFM measurements, we recorded $J-V$ curves on a minimum of five different regions of the sample to eliminate the effects of local heterogeneities for comparison to bulk device data. The $J-V$ curves from each region were averaged, resulting in a relative standard deviation of the mean (RSDM) of 15%.

The P3HT data in Figure 1 is representative of all polymers and tips used, in that the current densities obtained in c-AFM measurements are always significantly higher than those for the corresponding planar devices. The straight dotted lines in Figure 1 are fits of eq 1 to the experimental data. For our bulk device measurements on P3HT, the fits give an average hole mobility of 8.3×10^{-5} cm^2 V^{-1} s^{-1} (Table 1), which is in good agreement with values reported in the literature for SCLC mobility measurements made under similar conditions ($\mu_0 = 1.3 \times 10^{-5} - 3.3 \times 10^{-4}$ cm^2 V^{-1} s^{-1}).[37] However, depending on the sample, fits of eq 1 to the c-AFM measurements yield mobility values that are 50−4000 times larger than those obtained from the device measurements. The exact ratio depends on both the sample thickness and the tip diameter, irrespective of which polymer is used. These results are summarized in Table 2 for P3HT (see Supporting Information Table SI 1 for a complete tabulation).

The data in Table 2 led us to hypothesize that the current density obtained in a c-AFM experiment might exhibit a different dependence on the sample thickness than the current density obtained in a planar device. This result suggests that while SCLC measurements performed with the c-AFM may exhibit the V^2 dependence expected from eq 1; they likely deviate from the predicted $J \propto L^{-3}$ dependence. We test this explicitly in Figure 2, which shows the current density measured at 4 V from a set of c-AFM (Pt tip) and planar device measurements on P3HT as a function of sample thickness on a log−log scale. The current density for each

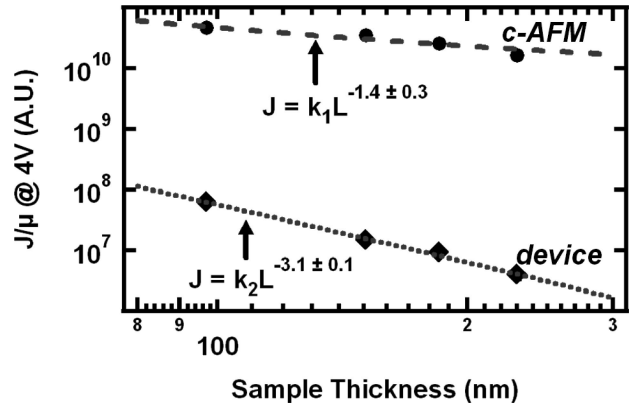

Figure 2. Current density relative to mobility as a function of sample thickness for both c-AFM (Pt tips) and device measurements on P3HT. The devices exhibit $J \propto L^{-3}$ behavior, as expected from eq 1. However, the c-AFM measurements deviate from this, showing approximately $J \propto L^{-1.4}$.

sample is divided by the carrier mobility in order to normalize the data for any sample-to-sample variations in mobility resulting from variations in polymer processing conditions. The dotted line in Figure 2 is a power law fit to the planar device data giving $J \propto L^{-3.1 \pm 0.1}$, in good agreement with the $J \propto L^{-3}$ relationship expected for SCLC in a planar geometry as predicted by eq 1. In contrast, when we fit a power law to the c-AFM data using Pt tips (dashed line), we obtain $J \propto L^{-1.4 \pm 0.3}$.

Fits of eq 1 have been used to extract hole mobilities from c-AFM data in a number of recent papers.[29,31,33,34,36] However, the deviation from the L^{-3} dependence of eq 1 clearly demonstrates that the unmodified Mott−Gurney law should not be used to extract mobilities from SCLC ($J-V$) data taken using c-AFM, even if J is proportional to V^2. While some reports have noted a discrepancy between the mobilities measured using fits to c-AFM data and the accepted bulk values,[29,33] this phenomena has yet to be explained quantitatively. Existing hypotheses for the discrepancy in the mobility include tip-induced injection enhancement[33] and "nanoscale confinement effects",[29] although both authors noted that the geometry of the measurement might be important. In the remainder of this paper, we attempt to explain the enhancement in current density observed in c-AFM relative to device measurements to facilitate quantitative measurements of local mobility using c-AFM.

The most obvious difference between SCLC measurements made using c-AFM and those using planar devices is the electrode geometry. Indeed, Kemerink and co-workers have emphasized the importance of considering the full three-dimensional (3D) geometry in the closely related problem of scanning tunneling spectroscopy and STM imaging on organic semiconductors.[25] Herein, we consider the SCLC case in limits relevant for c-AFM measurements on films with thicknesses similar to those used in devices. We extract a new scaling relationship that allows for the accurate interpretation of c-AFM $J-V$ curves without explicit numerical modeling of every sample. Figure 3 shows a cross-sectional diagram of the geometry in planar device and c-AFM experiments, illustrating the dramatic difference

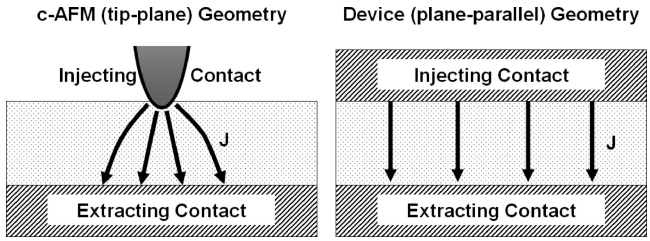

Figure 3. Schematics showing the c-AFM and device measurements' respective geometry. Two features may enhance SCLC density in c-AFM geometry. The current spreads out beneath the AFM tip allowing a larger space charge limited current density than is expected in the plane−parallel case.

Table 3. Example Mobility Values Obtained by Fitting Eq 2 to the Calculated Device and cAFM $J-V$ Curves[a]

AFM tip	L (nm)	μ_{device} [cm^2 V^{-1} s^{-1}]	$\mu_{c\text{-}AFM}$ [cm^2 V^{-1} s^{-1}]	$\mu_{c\text{-}AFM}/\mu_{device}$
platinum	185	2.53×10^{-5}	9.84×10^{-3}	389
	97	2.59×10^{-5}	3.21×10^{-3}	124
diamond	194	1.01×10^{-4}	1.16×10^{-3}	12
	125	8.51×10^{-5}	5.66×10^{-4}	7

[a] As in our experiments, the values of carrier mobility we obtain from the c-AFM data are much larger than for the planar devices, following the same trend with sample thickness and tip diameter. The input mobilities for these simulations are reported in Table 2.

between them. We hypothesize that the tip−plane electrode geometry of c-AFM experiments fundamentally alters the SCLC density from what we expect in the conventional case of planar electrodes. This hypothesis would explain both the deviation of our c-AFM experiments from the $J \propto L^{-3}$ relationship of eq 1 and the difference in the magnitude of the current density. Indeed, dimensional arguments and previous computational work on SCLCs[43–45] indicate a deviation from the L^{-3} dependence of the current density should be expected when the electrode geometry is changed from the planar device configuration. Grinberg et al.[45] showed that the current density between two thin strip electrodes scales as $J \propto L^{-2}$, and Atten et al.[44] reported $J \propto L^{-1}$ for a needle-plane geometry, as suggested by our observations.

In order to test this hypothesis, we performed numerical simulations of SCLCs in device and c-AFM geometries, by solving the coupled continuity equation (eq 3) and Poisson's equation (eq 4) for each case:

$$\frac{-\mathrm{d}\rho}{\mathrm{d}t} = \nabla \cdot (\mu\rho \nabla V + D\nabla\rho) \tag{3}$$

$$-\nabla^2 V = \frac{\rho}{\varepsilon\varepsilon_0} \tag{4}$$

where ρ is the charge density, t is time, ϵ is the relative dielectric constant of the active layer, ϵ_0 is the permittivity of free-space, μ is the charge carrier mobility, and V is the local electric potential (see Supporting Information for complete details). We solved the coupled eqs 3 and 4 using the finite element method (FEM), implemented in COMSOL Multiphysics (version 3.3a). This software allowed us to obtain solutions for potential and charge density distributions in relatively complex geometries. For devices, we used a one-dimensional (plane−parallel) model, while we modeled the c-AFM measurements in 3D with cylindrical symmetry.

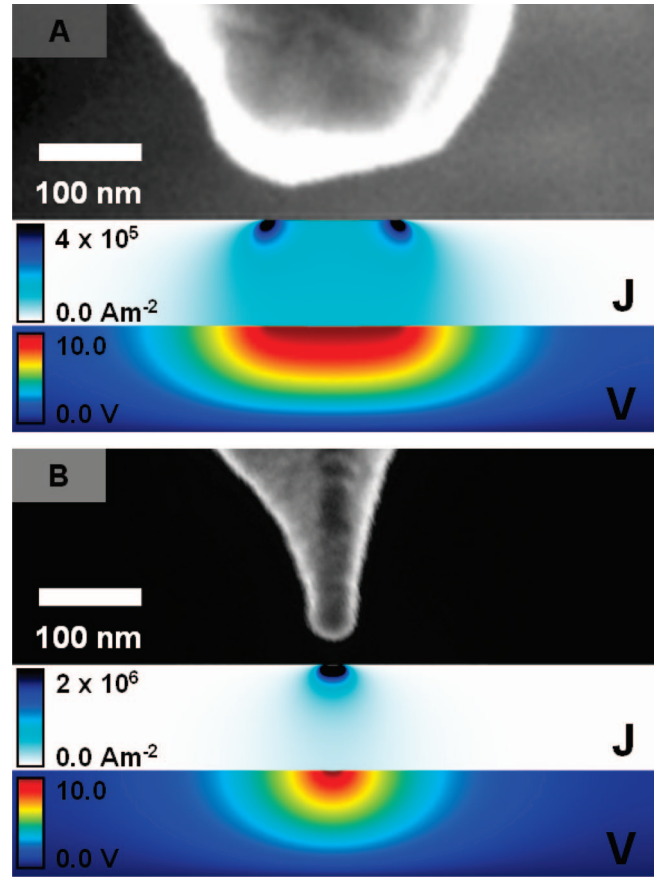

Figure 4. Example SEM images of diamond (A) and platinum (B) coated AFM tips used to make $I-V$ measurements. Two-dimensional slices of the corresponding numerical simulations are shown below each image, including the z component of the current density (J) distribution and the electrostatic potential (V).

As input to the calculations, we used the film thicknesses as measured via AFM and the experimental mobility values obtained from fits of eq 2 to the planar hole-only device data. We set $\varepsilon = 3$[46] and took the tip−sample contact area as 154 nm^2 ($d = 14$ nm) for the Pt tip, and 12 272 nm^2 ($d = 125$ nm) for the diamond tip, in agreement with SEM imaging of the actual tips used to collect the data in Figure 1. Figure 4A,B shows SEM images of the diamond- and platinum-coated AFM tips used in this set of experiments, respectively. While the tips are pyramidal in shape, we approximated them as circular contact patches in our model in order to make use of cylindrical symmetry in the computation. The ∼1 nm penetration depth for the tips is consistent with expectations from a simple Hertzian contact model assuming Young's modulus of ∼1 GPa for P3HT.[47] A shallow tip penetration depth is also consistent with our ability to image the polymer topography using c-AFM without observable surface damage. However, different penetration depths can be used without a strong effect on the current measured in c-AFM experiments. From our calculations, we expect less than ∼50% variation in total current for tip penetration depths between 1 and 10 nm (see Supporting Information Figures SI 7 and 8). Figure 4A,B shows the current density and potential profiles calculated from the SCLC simulations. As expected, the current density is high near the AFM tip and drops rapidly

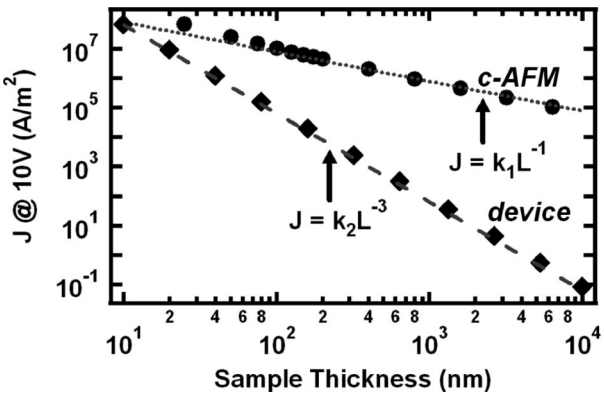

Figure 5. Calculated current density at 10 V tip bias for c-AFM and device geometries. In the limit of thick samples, the c-AFM calculation follows $J \propto L^{-1}$, but as L decreases, the calculation deviates toward a steeper slope. The calculations in device geometry follow $J \propto L^{-3}$ for the entire range, consistent with eq 1. These trends are in good agreement with our experimental observations in Figure 2.

to lower densities as the charge carriers spread out toward the planar electrode. This spreading of the current density beneath the tip challenges the common assumption that tip−apex diameter determines the resolution in c-AFM experiments. In fact, a much larger volume of the sample is probed, leading to an estimated resolution of ∼120, for a 100 nm thick film (see Supporting Information Figure SI 5). Nevertheless, there are many interesting fluctuations in local transport on these length scales that affect bulk device performance and are not accessible with other techniques.

Returning to the discrepancy in current density between measurements on the planar devices with c-AFM, our calculations suggest that properly accounting for the electrode geometry could explain both the altered sample thickness dependence and most of the difference in the magnitude of the current density. Figure 5 plots the calculated current density versus sample thickness for both c-AFM and planar device geometries. As expected, the calculated results for the planar device geometry follow the $J \propto L^{-3}$ predicted by eq 1. In contrast, and in good agreement with similar geometries in the literature,[44] the calculations for the c-AFM geometry show $\sim J \propto L^{-1}$ dependence for sample thicknesses greater than ∼500 nm. However, over the experimentally relevant range of sample thicknesses from ∼50−300 nm, Figure 5 shows the thickness dependence of the current density is approximately $J \propto L^{-1.4}$, which is consistent with our experimental data in Figure 2.

We next consider the ratio of the calculated current density in the planar device and c-AFM geometries. Figure 6A shows calculated $J-V$ curves for both geometries for a 185 nm thick P3HT sample with a mobility of 2.12×10^{-5} cm^2 V^{-1} s^{-1} (corresponding to the experimental data in Figure 1A); Figure 6B−D are analogous calculations corresponding to the experimental data in Figure 1B−D. The dotted lines in Figure 6 are fits of eq 1 to the simulated $J-V$ curves, and Table 2 summarizes the "mobility" values we obtained from fitting eq 1 to the simulated $J-V$ curves. Comparing the simulated values in Table 3 to our experimental values in Table 2, we see that the ratio of mobilities ($\mu_{\text{c-AFM}}/\mu_{\text{device}}$) from our calculations range from 7 to 400, depending on the details of tip sharpness and sample thickness, in good qualitative agreement with the experimental trends summarized in Table 2. The altered electrode geometry substantially changes the space charge limit of the current density at the AFM tip, yielding strongly enhanced current densities at the tip and a weakened dependence of J on sample thickness.

We can understand the impact of altered electrode geometry in terms of the freedom charge carriers have to spread out laterally as they travel from the injecting to extracting contact. In the case of a planar device, transport is effectively one-dimensional because of the uniformity of the electric field and charge density parallel to the electrodes. In contrast, transport between a tip and a planar substrate is three-dimensional, with current and charge density spreading significantly away from the tip (although ∼70% is localized within a ∼60 nm radius area from the tip for a 100 nm thick sample [Figure SI 5]).

These results seem to confirm our hypothesis that accounting for the tip−sample geometry can explain the enhanced current density and altered thickness dependence observed in SCLC measurements performed with c-AFM. Our results for P3HT show a factor of $\sim 7.8 \pm 1$ by which our calculations underestimate the observed current density in c-AFM experiments. However, the trends in the variation of current density with sample thickness and tip diameter are reproduced almost exactly, and they allow us to improve the agreement between c-AFM and planar device measurements by nearly 3 orders of magnitude. We thus conclude that geometry accounts for most of the difference between c-AFM and planar SCLC measurements. The relatively constant offset between simulation and experiment suggests that we can use our finite element calculations to fit $J-V$ curves obtained using c-AFM to quantitatively determine local charge carrier mobilities by taking the offset factor we observe into account as an empirical parameter. However, it is inconvenient to run a numerical simulation whenever one wishes to calculate mobility from a $J-V$ curve taken using c-AFM. What we require is a simple semiempirical modification to eqs 1 and 2 that will allow us to fit c-AFM $J-V$ curves directly and accurately determine the carrier mobility. The ratio of mobilities ($\mu_{\text{c-AFM}}/\mu_{\text{device}}$) shown in Tables 2 and 3 provides a convenient "mobility correction factor" for this purpose.

Figure 7A plots the mobility correction factor ($\mu_{\text{c-AFM}}/\mu_{\text{device}}$) against the ratio of estimated tip contact area diameter to sample thickness, d/L, where d is the diameter of the (circular) tip−sample contact area and L is the sample thickness. The experimental data for P3HT is plotted as open green circles, and the calculations appear as filled squares. Notably, we obtain a good agreement only when scaling versus d/L: if we try to plot the mobility ratio as a function of sample thickness alone (P3HT, inset), tips of differing diameter (Pt vs diamond) do not follow the same curve. For convenience, we fit a power law to the calculations over the range of our experimental data (dotted lines in Figure 7A) in order to obtain an approximate expression for the mobility

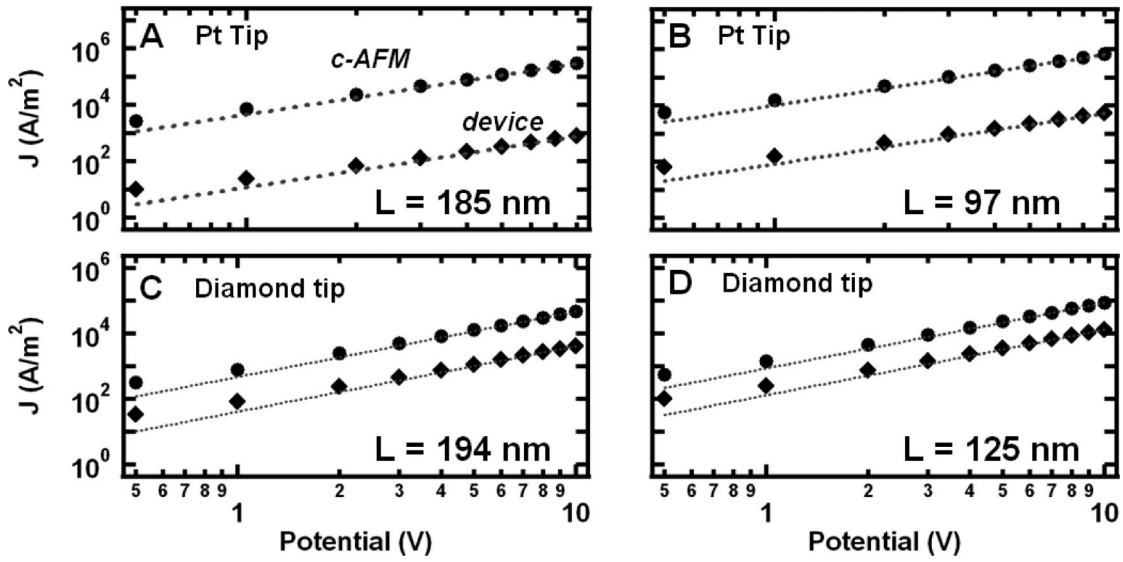

Figure 6. Calculated $J-V$ curves for both cAFM (circles) and device (diamonds) geometries. In each case, the mobility extracted from the corresponding device measurement was used as the simulation input (Table 2). In all cases, the c-AFM results exhibit larger current densities, despite the same intrinsic mobility.

scaling factor as a function of d/L, resulting in an exponent of -1.6 ± 0.1. This is consistent with our observation of an intermediate thickness dependence of the current density for sample thicknesses within the experimentally relevant regime where the tip diameter is roughly comparable to the sample thickness. The success of applying our scaling factor relative to the Mott−Gurney law is shown for the P3HT data in Figure 7B,C. Figure 7B plots the ratio of the current density measured using c-AFM to the mobility (bulk) of each sample using the L^{-3} thickness scaling predicted by eq 1. In contrast, Figure 7C shows the curves after scaling by our additional factor of $(d/L)^{-1.6}$. Figure 7C is a key result of this paper as it shows that we can successfully scale curves varying by over 3 orders of magnitude in J onto a single curve (mobility value) independent of the sample thickness and tip diameter.

Using our expression for the mobility scaling factor to modify eq 2, we propose a semiempirical expression for the current density measured in a c-AFM electrode geometry:

$$J = \alpha\varepsilon\varepsilon_0\mu_0 e^{0.89\gamma(V/L)^{1/2}}\frac{V^2}{L^3}\delta\left(\frac{L}{d}\right)^{1.6\pm0.1} \quad (5)$$

where α is the prefactor determined from our numerical calculations to have a value of ~8.2 (in place of 9/8 from the Mott−Gurney law), δ is an empirical dimensionless parameter accounting for the offset between c-AFM calculations and the P3HT data, d is the estimated diameter of the tip−substrate contact area, $J_{c\text{-AFM}}$ is the average current density at the AFM tip normal to the extracting plane, ϵ is the relative dielectric constant of the active layer, ϵ_0 is the permittivity of free space, μ is the charge carrier mobility, V is the applied voltage, γ expresses the apparent field dependence (or charge density dependence) of the mobility ($\gamma = 0$ for P3HT), and L is the active layer thickness. When we fit our power law expression for the mobility correction factor to the calculation and experimental data for P3HT, as shown by the dashed lines in Figure 7A, we obtain a value of $\delta = 7.8 \pm 1$. We expect that this value of δ will be applicable to sample thicknesses and tip contact area diameters in the range of $0.01 \leq d/L \leq 2$, since eq 5 is consistent with our numerical model to within 50% over this interval. Table 4 shows examples of the mobilities we obtain by fitting our c-AFM $J-V$ curves taken on P3HT using eq 5. By using this value of δ, the hole mobility values measured using c-AFM agree with the bulk measurements to within a factor of 2 at worst for all P3HT samples, with an overall rms deviation of 6.2% from the bulk measurements.

Table 4. Example Mobility Fits to the cAFM Data Using Eq 5[a]

AFM tip	L (nm)	μ_{device} [$cm^2\ V^{-1}\ s^{-1}$]	$\mu_{c\text{-AFM}}$ [$cm^2\ V^{-1}\ s^{-1}$]	$\mu_{c\text{-AFM}}/\mu_{device}$
platinum	185	2.12×10^{-5}	2.18×10^{-5}	1.0
	97	2.19×10^{-5}	1.70×10^{-5}	0.8
diamond	194	8.45×10^{-5}	8.34×10^{-5}	1.0
	125	7.38×10^{-5}	7.68×10^{-5}	1.0

[a] For all P3HT films, the mobilities measured using c-AFM agrees with the planar device measurements to within a factor of 2. For all films, including PFB and MDMO-PPV, the agreement between c-AFM and device measurements agrees within a factor of 7.

To further test this model, we have also performed space charge limited current measurements on PFB and MDMO-PPV films in the planar device and c-AFM geometries (Supporting Information Tables SI 1 and 2). The results are generally consistent with the P3HT data and are plotted as orange squares and blue circles on Figure 7A for PFB and MDMO-PPV, respectively. However, there are differences worth noting. In particular, the thickness dependence appears even weaker in the MDMO-PPV and PFB samples. Nevertheless, it is much closer to the $L^{-1.4}$ we calculated in this intermediate thickness range ($0.01 \leq d/L \leq 2$) than the L^{-3} from the Mott−Gurney law. In addition, both the planar device and the c-AFM fits require the use of a field-dependent mobility parameters to properly fit the $J-V$ curves ($\gamma = 5.4 \times 10^{-4}$ and 7.2×10^{-4} for MDMO-PPV and PFB, respectively). Interestingly, there is a distinct trend in the slope of the data in Figure 7A with increasing γ factor, suggesting that a stronger apparent field-dependence of the

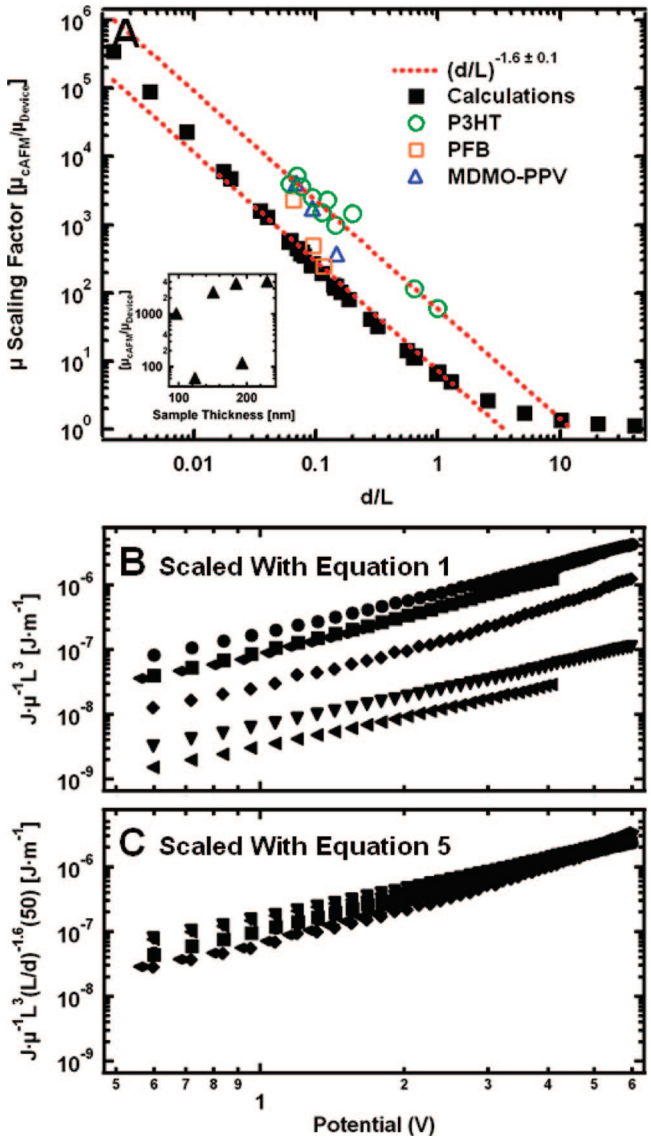

Figure 7. (A) "Mobility ratio" or "scaling factor" vs the ratio of AFM tip diameter to effective sample thickness. The inset shows the mobility scaling factor for our P3HT data as a function of sample thickness alone. Our calculations are shown as filled squares, and the experimental data are shown as open markers with green circles, orange squares, and blue triangles for P3HT, PFB, and MDMO-PPV, respectively. (B) Current density relative to bulk mobility measured using c-AFM on P3HT samples scaled for sample thickness using eq 1. The different data markers indicate different thicknesses and tip diameters. (C) Current density relative to bulk mobility of each P3HT sample, scaled for sample thickness and tip diameter using eq 5.

mobility will lead to less accurate values of the mobility obtained with equation 5. Nevertheless, when using eq 5 to fit the $J-V$ curves for MDMO-PPV and PFB, the local and bulk mobilities all agree within an order of magnitude (a factor of 7 is the worst discrepancy) which is a 100-fold improvement upon fitting with the simple Mott−Gurney law. Again, this result supports our contention that the tip−sample geometry is the main factor leading to discrepancy between c-AFM and planar device measurements.

We believe that eq 5 will prove to be useful for analysis of c-AFM data from a variety of semiconducting polymers. While the scaling in eq 5 can improve the accuracy of a c-AFM measurement by a factor of 100−1000, we note that several features of the experiment and calculation remain unexplained. In particular, the origin of the empirical factor δ and the d/L scaling changes in materials with field-dependent mobilities remain open questions. Some discrepancy is probably expected, given the experimental errors and computational approximations involved. Although we measured our AFM tips using SEM, there remains some possibility for systematic experimental error in our estimates of tip−sample contact area and tip penetration depth. Computationally, discrepancies could arise because of our approximation of the pyramidal tips as circular contact patches, our treatment of the problem assuming hole-only transport, and our assumption of constant mobility (with respect to charge density and electric field). We have investigated each possibility, including an analysis of tip−sample contact forces, tip penetration, variable mobility, and tip shape (Supporting Information). Although we are unable to attribute the value of δ to any single factor, we show (Figure SI 4A,B) that including a charge density-dependent mobility in the simulation has the greatest success in explaining this discrepancy, and we suggest that our assumption of constant charge carrier mobility may be a significant factor in the remaining disagreement between our experiments and calculations. The trend in the slope of the data in Figure 7A with increasing γ values supports this hypothesis and shows that a field- or charge density-dependent mobility can impact the comparison between c-AFM and device experiments. We suggest that once the field- and/or charge density-dependence of carrier mobility in different organic semiconductors is better understood, it may be possible to achieve even better quantitative agreement between simulations and experimental measurements of c-AFM currents. As a corollary, because of their deviations from the planar geometry, c-AFM measurements may provide more sensitive tests of different microscopic transport models than planar device measurements.

In summary, several studies have reported a large discrepancy between the current density (and thus the calculated charge carrier mobility) measured with c-AFM and that measured with a macroscopic planar device. We have shown that the primary cause of this observation is the difference in geometry between the two experiments. The typical one-dimensional analysis of space charge limited $J-V$ curves using eqs 1 and 2 is not appropriate for c-AFM measurements because SCLC measurements performed with c-AFM deviate from the $J \propto L^{-3}$ dependence expected from the one-dimensional Mott−Gurney law. We propose a semiempirical equation (eq 5) which is valid for common tip diameters and sample thicknesses, using a scaling factor based on the ratio of tip diameter to sample thickness. This scaling factor collapses a range of experimental data onto a single curve and can be used to extract quantitative values of charge carrier mobility from $J-V$ curves collected by c-AFM for samples with weakly field- or charge density-dependent mobilities. Through this procedure, we have reduced the discrepancy between mobilities measured in devices and with

c-AFM by over 3 orders of magnitude in some cases. These results should allow the measurement of local mobility with nanoscale resolution in heterogeneous polymer films used in light-emitting diodes, transistors, and solar cells. Nevertheless, some quantitative discrepancies remain, and future work incorporating more refined descriptions of the field- or charge density-dependent mobility into modeling of c-AFM currents may yield even better agreement.

Acknowledgment. This paper is based on work supported by the National Science Foundation (DMR 0449422) and the STC program of the National Science Foundation (DMR 0120967). D.S.G. also thanks the Camille Dreyfus Teacher-Scholar Awards Program for support. D.S.G. is a Cottrell Scholar of the Research Corporation and an Alfred P. Sloan Foundation Research Fellow. O.G.R. acknowledges that this research was supported by the Center for Nanotechnology at the UW with funding from an IGERT Fellowship Award NSF #DGE-0504573. We thank Martijn Kemerink for supplying us with a copy of his code[25] and providing assistance in getting it running which we used to compare against our COMSOL model. We thank Deanna B. Rodovsky and Professor Lee Y. Park for synthesizing our stock of MDMO-PPV.

Note Added after ASAP Publication: There was an error in Table 1 in the version of this paper published ASAP May 1, 2008; the corrected version was published ASAP May 16, 2008.

Supporting Information Available: We provide a complete description of our numerical simulations, and the impact of variable mobility (depending on electric field or charge density). We show a complete tabulation of data from all of the different tip materials and polymers used. We determine the total contact force in our $I-V$ measurements using c-AFM and discuss the probable extent and effects of tip penetration. Finally, we provide a theoretical estimate for the spatial resolution of our mobility measurements. This material is available free of charge via the Internet at http://pubs.acs.org.

References

(1) Shaheen, S. E.; Ginley, D. S.; Jabbour, G. E. *MRS Bull.* **2005**, *30* (1), 10–19.
(2) Nelson, J. *Science* **2001**, *293* (5532), 1059–1060.
(3) Kelley, T. W.; Baude, P. F.; Gerlach, C.; Ender, D. E.; Muyres, D.; Haase, M. A.; Vogel, D. E.; Theiss, S. D. *Chem. Mater.* **2004**, *16* (23), 4413–4422.
(4) Sirringhaus, H.; Tessler, N.; Friend, R. H. *Science* **1998**, *280* (5370), 1741–1744.
(5) Mayer, A. C.; Scully, S. R.; Hardin, B. E.; Rower, M. W.; McGehee, M. D. *Materials Today* **2007**, *10* (11), 28–33.
(6) Shaheen, S. E.; Brabec, C. J.; Sariciftci, N. S.; Padinger, F.; Fromherz, T.; Hummelen, J. C. *Appl. Phys. Lett.* **2001**, *78* (6), 841–843.
(7) Kim, Y.; Choulis, S. A.; Nelson, J.; Bradley, D. D. C.; Cook, S.; Durrant, J. R. *Appl. Phys. Lett.* **2005**, *86* (6).
(8) Ma, W. L.; Yang, C. Y.; Gong, X.; Lee, K.; Heeger, A. J. *Adv. Funct. Mater.* **2005**, *15* (10), 1617–1622.
(9) Li, G.; Shrotriya, V.; Huang, J. S.; Yao, Y.; Moriarty, T.; Emery, K.; Yang, Y. *Nat. Mater.* **2005**, *4* (11), 864–868.
(10) Coakley, K. M.; McGehee, M. D. *Chem. Mater.* **2004**, *16* (23), 4533–4542.
(11) Sirringhaus, H.; Wilson, R. J.; Friend, R. H.; Inbasekaran, M.; Wu, W.; Woo, E. P.; Grell, M.; Bradley, D. D. C. *Appl. Phys. Lett.* **2000**, *77* (3), 406–408.
(12) Shi, Y.; Liu, J.; Yang, Y. *J. Appl. Phys.* **2000**, *87* (9), 4254–4263.
(13) Blom, P. W. M.; Mihailetchi, V. D.; Koster, L. J. A.; Markov, D. E. *Adv. Mater.* **2007**, *19*, 1551–1566.
(14) Blom, P. W. M.; de Jong, M. J. M.; Liedenbaum, C. *Polym. Adv. Technol.* **1998**, *9* (7), 390–401.
(15) Smits, E. C. P.; Mathijssen, S. G. J.; Colle, M.; Mank, A. J. G.; Bobbert, P. A.; Blom, P. W. M.; de Boer, B.; de Leeuw, D. M. *Phys. Rev. B* **2007**, *76* (12), 125202. (1−5)
(16) Marsh, R. A.; Groves, C.; Greenham, N. C. *J. Appl. Phys.* **2007**, *101* (8), 083509. (1−7)
(17) Rappaport, N.; Solomesch, O.; Tessler, N. *J. Appl. Phys.* **2006**, *99* (6), 064507. (1−5)
(18) Rappaport, N.; Bar, Y.; Solomeshch, O.; Tessler, N. *Appl. Phys. Lett.* **2006**, *89* (25), 252117. (1−3)
(19) Frost, J. M.; Cheynis, F.; Tuladhar, S. M.; Nelson, J. *Nano Lett.* **2006**, *6* (8), 1674–1681.
(20) Athanasopoulos, S.; Kirkpatrick, J.; Martinez, D.; Frost, J. M.; Foden, C. M.; Walker, A. B.; Nelson, J. *Nano Lett.* **2007**, *7* (6), 1785–1788.
(21) Coffey, D. C.; Ginger, D. S. *Nat. Mater.* **2006**, *5* (9), 735–740.
(22) Chiesa, M.; Burgi, L.; Kim, J. S.; Shikler, R.; Friend, R. H.; Sirringhaus, H. *Nano Lett.* **2005**, *5* (4), 559–563.
(23) Hoppe, H.; Glatzel, T.; Niggemann, M.; Hinsch, A.; Lux-Steiner, M. C.; Sariciftci, N. S. *Nano Lett.* **2005**, *5* (2), 269–274.
(24) Silveira, W. R.; Marohn, J. A. *Phys. Rev. Lett.* **2004**, *93* (11), 116104. (1−4)
(25) Kemerink, M.; Alvarado, S. F.; Muller, P.; Koenraad, P. M.; Salemink, H. W. M.; Wolter, J. H.; Janssen, R. A. J. *Phys. Rev. B: Condens. Matter Mater. Phys.* **2004**, *70* (4), 045202. (1−13)
(26) Kemerink, M.; Timpanaro, S.; de Kok, M. M.; Meulenkamp, E. A.; Touwslager, F. J. *J. Phys. Chem. B* **2004**, *108* (49), 18820–18825.
(27) Nardes, A. M.; Kemerink, M.; Janssen, R. A. J.; Bastiaansen, J. A. M.; Kiggen, N. M. M.; Langeveld, B. M. W.; van Breemen, A.; de Kok, M. M. *Adv. Mater.* **2007**, *19* (9), 1196–1200.
(28) Pingree, L. S. C.; Hersam, M. C.; Kern, M. M.; Scott, B. J.; Marks, T. J. *Appl. Phys. Lett.* **2004**, *85* (2), 344–346.
(29) Lin, H. N.; Lin, H. L.; Wang, S. S.; Yu, L. S.; Perng, G. Y.; Chen, S. A.; Chen, S. H. *Appl. Phys. Lett.* **2002**, *81* (14), 2572–2574.
(30) Liau, Y. H.; Scherer, N. F.; Rhodes, K. *J. Phys. Chem. B* **2001**, *105* (16), 3282–3288.
(31) Ionescu-Zanetti, C.; Mechler, A.; Carter, S. A.; Lal, R. *Adv. Mater.* **2004**, *16* (5), 385–389.
(32) Alexeev, A.; Loos, J.; Koetse, M. M. *Ultramicroscopy* **2006**, *106* (3), 191–199.
(33) Douheret, O.; Lutsen, L.; Swinnen, A.; Breselge, M.; Vandewal, K.; Goris, L.; Manca, J. *Appl. Phys. Lett.* **2006**, *89* (3), 032107. (1−3)
(34) Douheret, O.; Swinnen, A.; Breselge, M.; Van Severen, I.; Lutsen, L.; Vanderzande, D.; Manca, J. *Microelectron. Eng.* **2007**, *84* (3), 431–436.
(35) (a) Coffey, D. C.; Ginger, D. S. *J. Am. Chem. Soc.* **2005**, *127* (13), 4564−4565. (b) Coffey, D. C.; Reid, O. G.; Rodovsky, D. B.; Bartholomew, G. P.; Ginger, D. S. *Nano Lett.* **2007**, *7*, 738−744. (c) Pingree, L. S. C.; MacLeod, B. A.; Ginger, D. S. *J. Phys. Chem. C* ASAP Article, DOI: 10.1021/jp711838h.
(36) Yang, R. Q.; Garcia, A.; Korystov, D.; Mikhailovsky, A.; Bazan, G. C.; Nguyen, T. Q. *J. Am. Chem. Soc.* **2006**, *128* (51), 16532–16539.
(37) Goh, C.; Kline, R. J.; McGehee, M. D.; Kadnikova, E. N.; Frechet, J. M. J. *Appl. Phys. Lett.* **2005**, *86* (12), 122110. (1−3)
(38) Mozer, A. J.; Sariciftci, N. S. *Chem. Phys. Lett.* **2004**, *389* (4−6), 438–442.
(39) Blom, P. W. M.; deJong, M. J. M.; vanMunster, M. G. *Phys. Rev. B* **1997**, *55* (2), R656–R659.
(40) Tanase, C.; Blom, P. W. M.; de Leeuw, D. M. *Phys. Rev. B* **2004**, *70* (19), 193202. (1−4)
(41) Murgatroyd, P. N. *J. Phys. D: Appl. Phys.* **1970**, *3* (2), 151–157.
(42) Pasveer, W. F.; Cottaar, J.; Tanase, C.; Coehoorn, R.; Bobbert, P. A.; Blom, P. W. M.; de Leeuw, D. M.; Michels, M. A. J. *Phys. Rev. Lett.* **2005**, *94* (20), 206601. (1−4)
(43) Hare, R. W.; Hill, R. M. *J. Phys. D: Appl. Phys.* **1991**, *24* (3), 398–406.
(44) Atten, P.; Adamiak, K.; Khaddour, B.; Coulomb, J. L. *J. Optoelectron. Adv. Mater.* **2004**, *6* (3), 1023–1028.
(45) Grinberg, A. A.; Luryi, S.; Pinto, M. R.; Schryer, N. L. *IEEE Trans. Electron Devices* **1989**, *36* (6), 1162–1170.
(46) Blom, P. W. M.; deJong, M. J. M.; Vleggaar, J. J. M. *Appl. Phys. Lett.* **1996**, *68* (23), 3308–3310.
(47) Miyauchi, S.; Kondo, T.; Oshima, K.; Yamauchi, T.; Shimomura, M.; Mitomo, H. *J. Appl. Polym. Sci.* **2002**, *85* (7), 1429–1433.

NL080155L